

Charge distribution induced inside complex plasmonic nanoparticles

R. Marty¹, G. Baffou², A. Arbouet¹, C. Girard¹, and R. Quidant^{2,3}

¹*CEMES, CNRS, Université Paul Sabatier, 29 rue Jeanne Marvig 31055 Toulouse, France*

²*ICFO-Institut de Ciències Fotòniques, 08860 Castelldefels (Barcelona), Spain*

³*ICREA-Institució Catalana de Recerca i Estudis Avançats, 08010 Barcelona, Spain*

Corresponding author: girard@cemes.fr

Abstract: We developed a versatile numerical technique to compute the three-dimensional charge distribution inside plasmonic nanoparticles. This method can be easily applied to investigate the charge distribution inside arbitrarily complex plasmonic nanostructures and to identify the nature of the multipolar plasmon modes involved at plasmonic resonances. Its ability to unravel the physical origin of plasmonic spectral features is demonstrated in the case of a single gold nanotriangle and of a gold nano-antenna. Finally, we show how the volume charge distribution can be used to define and compute the first terms of the multipolar expansion.

© 2010 Optical Society of America

OCIS codes: (000.0000) General.

References and links

1. U. Kreibig and M. Vollmer, *Optical properties of metal clusters* (Springer-Verlag, Berlin, 1995).
2. A. Drezet, A. Hohenau, J. R. Krenn, M. Brun and S. Huan, "Surface plasmon mediated near field imaging and optical addressing in nanoscience," *Micron* **38**, 427 (2007).
3. E. K. Payne, K. L. Shuford, S. Park, G. C. Schatz and C. A. Mirkin, "Multipole plasmon resonances in gold nanorods," *J. Phys. Chem. B* **110**, 2150 (2006).
4. K. L. Shuford, M. A. Ratner, and G. C. Schatz, "Multipolar excitation in triangular nanoprisms," *J. Chem. Phys.*, **123**, 114713 (2005)
5. J. R. Krenn, G. Schider, W. Rechberger, B. Lamprecht, A. Leitner and F. R. Aussenegg, "Design of multipolar plasmon excitations in silver nanoparticles," *Appl. Phys. Lett.* **77**, 3379 (2000).
6. L. J. Sherry, R. Jin, C. A. Mirkin, G. C. Schatz and R. P. Van Duyne, "Localized Surface Plasmon Resonance Spectroscopy of single silver triangular nanoprisms," *Nano Lett.* **6**, 2060 (2006).
7. N. Féliđj, J. Grand, G. Laurent, J. Aubard, G. Lévi, A. Hohenau, N. Galler, F. R. Aussenegg and J. R. Krenn, "Multipolar surface plasmon peaks on gold nanotriangles," *J. Chem. Phys.* **128**, 094702 (2008).
8. S. J. Oldenburg, G. D. Hale, J. B. Jackson, and N. J. Halas, "Light Scattering from dipole and quadrupole nanoshell antennas," *Appl. Phys. Lett.* **75**, 1063 (1999).
9. J. Nelayah, M. Kociak, O. Stephan, F. J. Garcia de Abajo, M. Tencé, L. Henrard, D. Taverna, I. Pastoriza-Santos, L. M. Liz-Marazán and C. Colliex, "Mapping surface plasmons on a single metallic nanoparticle," *Nat. Phys.* **3**, 348 (2007).
10. J. P. Kottmann and O. J. F. Martin, "Plasmon resonant coupling in metallic nanowires," *Opt. Express* **8**, 655 (2001).
11. J. P. Kottmann, O. J. F. Martin, D. R. Smith and S. Schultz, "Field polarization and polarization charge distributions in plasmon resonant nanoparticles," *New J. Phys.* **2**, 27.1 (2000).
12. M. Liu, T. Lee, S. K. Gray, P. Guyot-Sionnest and M. Pelton, "Excitation of dark plasmons in metal nanoparticles by a localized emitter," *Phys. Rev. Lett.* **102**, 107401 (2009).
13. H. Wang, Y. Wu, B. Lassiter, C. L. Nehl, J. H. Hafner, P. Nordlander and N. J. Halas, "Symmetry breaking in individual plasmonic nanoparticles," *PNAS* **103**, 10856 (2006).

14. A. Christ, O. J. F. Martin, Y. Ekinici, N. A. Gippius, S. G. Tikhodeev, "Symmetry breaking in a plasmonic metamaterial at optical wavelength," *Nano Lett.* **8**, 2171 (2008).
15. N. Verellen, Y. Sonnefraud, H. Sobhani, F. Hao, V. V. Moshchalkov, P. Van Dorpe, P. Nordlander and S. A. Maier, "Fano resonances in individual coherent plasmonic nanocavities," *Nano Lett.* **9**, 1663 (2009).
16. F. Hao, P. Nordlander, Y. Sonnefraud, P. Van Dorpe and S. A. Maier, "Tunability of subradiant dipolar and fano-type plasmon resonances in metallic ring/disk cavities : implications for nanoscale optical sensing," *ACS Nano* **3**, 643 (2009).
17. C. Ropers, D. J. Park, G. Stibenz, G. Steinmeyer, J. Kim, D. S. Kim and C. Lienau, "Femtosecond light transmission and subradiant damping in plasmonic crystals," *Phys. Rev. Lett.* **94**, 113901 (2005).
18. R. Fuchs, "Theory of the optical properties of ionic crystal cubes," *Phys. Rev. B* **11**, 1732 (1975).
19. F. J. Garcia de Abajo, "Retarded field calculation of electron energy loss in inhomogeneous dielectrics," *Phys. Rev. B* **65**, 115418 (2002).
20. C. Girard, "Near fields in nanostructures," *Rep. Prog. Phys.* **68**, 1883 (2005).
21. A. A. Lazarides, and G. C. Schatz, "DNA-Linked Metal Nanosphere Materials: Structural Basis for the Optical Properties," *J. Phys. Chem. B*, **104**, 460 (2000)
22. P. B. Johnson and R. W. Christy, "Optical constants of the noble metals," *Phys. Rev. B* **6**, 4370 (1972).
23. R. Jin, Y. Cao, C. A. Mirkin, K. L. Kelly, G. C. Schatz and J. G. Zheng, "Photoinduced conversion of silver nanospheres to nanoprisms," *Science* **294**, 1901 (2001).
24. K. L. Kelly, E. Coronado, L. L. Zhao, and G. C. Schatz, "The optical properties of metal nanoparticles : the influence of size, shape, and dielectric environment," *J. Phys. Chem. B* **107**, 668 (2003).
25. C. L. Haynes, A. D. McFarland, L. L. Zhao, R. P. Van Duyne and G. C. Schatz, "Nanoparticle optics : the importance of radiative coupling in two dimensional nanoparticle arrays," *J. Phys. Chem. B* **107**, 7337 (2003).
26. J. E. Millstone, S. Park, K. L. Shuford, L. Qin, G. C. Schatz and C. A. Mirkin, "Observation of a quadrupole plasmon mode for a colloidal solution of gold nanoprisms," *JACS* **127**, 5312 (2005).
27. M. Rang, A. C. Jones, F. Zhou, Z. Li, B. J. Wiley, Y. Xia and M. B. Raschke, "Optical near-field mapping of plasmonic nanoprisms," *Nano Lett.* **8**, 3357 (2008).
28. A. D. Buckingham, "Permanent and induced molecular moments and long-range intermolecular forces," *Adv. Chem. Phys.* **12**, 107 (1967).
29. C. Girard, "Multipolar propagators near a corrugated surface: Implication for local probe microscopy," *Phys. Rev. B* **45**, 1800 (1992).

1. Introduction

The linear optical properties of small metallic aggregates have been extensively investigated for the last fifty years. In the case of noble metal particles, characterized by a permittivity $\epsilon_m(\omega_0)$, embedded in transparent materials of dielectric constant ϵ_{em} , the interface between the two media introduces surface plasmon resonances, the frequency of which depends on the optical properties of the metal and the surroundings, as well as the topography of the particle surface [1]. In these systems, the resonant excitation of electron oscillations leads to a dramatic enhancement of the optical near-field simultaneously with a spatial localization of the electromagnetic energy in nanometer sized volumes[2].

For nanoparticles with sizes down to the optical wavelength, the surface plasmon resonances are clearly dipolar and can be satisfactorily described by the lowest order of the series of spherical harmonics of Mie theory. For larger particles, typically in the 100 nm range, retardation effects inside the plasmonic particles lead to the appearance of higher order multipolar plasmon resonances that show off as new features in the optical spectra [3, 4]. The spectral signatures of these higher order plasmon resonances have first been observed in elongated gold and silver nanoparticles either colloidal or lithographically fabricated [3, 5] and more recently in noble metal nanoprisms [4, 6, 7]. These multipolar modes have been identified through the size dependence of their spectral position [5] or the angular distribution of the scattered light [8]. Nevertheless, fewer experimental investigations have directly demonstrated the multipolar character of the observed resonances [9]. Theoretical studies of these multipolar resonances have been achieved in two-dimensional (2D) silver scatterers of arbitrary cross-sections [10] by computing and representing the induced surface charge density [11].

Recently, the specific properties of these multipolar plasmon resonances have attracted a lot of attention. Indeed, while the dipolar plasmon modes have a very high radiative damping rate

leading to prohibitive energy losses for their use in plasmonic nanodevices, the plasmon modes of higher orders display lower radiative losses since they couple weakly to an homogeneous external electric field. This property could make them interesting for carrying optical signals in plasmonic circuits composed of metallic particles assembled on a surface [12]. In a similar context, it has been shown that the optical activity of the high-order localized plasmon modes of plasmonic metamaterials can be enhanced by introducing a structural asymmetry [13, 14]. The coherent coupling between different plasmon modes leads to the appearance of a Fano-like line shape in the extinction spectrum of plasmonic nanocavities [15, 16]. In the time domain, the coherent coupling between different plasmon modes can be used to enhance dramatically the lifetime of coupled antisymmetric plasmon modes [17]. Consequently, the engineering of the high-order plasmon resonances of plasmonic nanostructures should bring significant breakthrough in plasmonic nano-devices and plasmonic circuitry.

In this context, a versatile tool is required to directly visualize the charge distribution inside complex plasmonic systems composed of one unit or several interacting subsystems. Boundary integrals or boundary element methods allows evaluating the surface charge density on the surface of arbitrarily shaped nano-objects. For instance, this has been shown by Fuchs in the case of ionic crystal cubes[18]. This approach has been recently extended to take into account retardation effects in arbitrarily shaped dielectrics by Garcia de Abajo *et al*[19]. However, to our knowledge, the full three dimensional volume charge density inside complex plasmonic nanostructures has not been computed yet. In this communication, we describe a theoretical scheme together with a numerical procedure to compute the volume charge distribution inside plasmonic nanoparticles of arbitrary shape. We demonstrate that the method is well-suited to the investigation of the charge repartition and to the identification of the multipolar plasmon modes inside complex plasmonic nanostructures. Its ability to unravel the physical origin of a spectral feature of a plasmonic nanoparticle is demonstrated with a single gold nanotriangle and a bow-tie gold nanoantenna. The first three lowest order multipole moments of the charge distribution are then computed.

2. Calculation of the charge distribution inside plasmonic nanoparticles: theory and numerical procedure

Majority of the numerical investigations of the optical response of metallic nanostructures is limited to the computation of the far-field properties (scattering, absorption and extinction cross-sections) or near-field intensity distribution. However, to support the continuous improvement of fabrication methods and experimental measurements, a deeper understanding of the physics of plasmonic structures also requires the direct visualization of the charge distribution induced inside single or interacting metal nanoparticles. To deal with this problem, we have developed the electro-dynamical theory of the field-susceptibilities [20] in order to gain access to the spatial repartition of the charges inside the metal. In this framework, we solve the Maxwell equations by writing the inhomogeneous wave equation:

$$\Delta \mathbf{E}(\mathbf{r}, \omega_0) + k^2 \mathbf{E}(\mathbf{r}, \omega_0) = -4\pi [k_0^2 + \frac{1}{\epsilon(\mathbf{r}, \omega_0)} \nabla \nabla] \cdot \mathbf{P}(\mathbf{r}, \omega_0), \quad (1)$$

where the vector $\mathbf{P}(\mathbf{r}, \omega_0)$ represents the electric polarization induced inside the materials, $k_0 = \omega_0/c$, and $k = \sqrt{\epsilon_{em}} k_0$. The field-susceptibility theory allows the general solution of Helmholtz equation (1) to be found:

$$\mathbf{E}(\mathbf{r}, \omega_0) = \mathbf{E}_0(\mathbf{r}, \omega_0) + \int_V \mathbf{S}_0(\mathbf{r}, \mathbf{r}', \omega_0) \cdot \mathbf{P}(\mathbf{r}', \omega_0) d\mathbf{r}', \quad (2)$$

where the electric field $\mathbf{E}_0(\mathbf{r}, \omega_0)$ verifies the homogeneous Helmholtz equation (in the absence of any nanostructure) and $\mathbf{S}_0(\mathbf{r}, \mathbf{r}', \omega_0)$ is the field-susceptibility tensor associated with the envi-

ronment. In the framework of the linear response theory, the relationship between local electric field and polarization inside the plasmonic nanostructure is given by:

$$\mathbf{P}(\mathbf{r}', \omega_0) = \chi(\mathbf{r}', \omega_0) \cdot \mathbf{E}(\mathbf{r}', \omega_0) \quad (3)$$

Assuming a local response of the material, the susceptibility $\chi(\mathbf{r}', \omega_0)$ can be written:

$$\chi(\mathbf{r}, \omega_0) = \frac{\epsilon_m(\mathbf{r}, \omega_0) - \epsilon_{env}}{4\pi} . \quad (4)$$

After substitution of equation (3) into relation (2), the Lippmann–Schwinger equation can be solved by meshing the investigated metallic nanostructure in a lattice of a total of N points located at positions \mathbf{r}_i . This procedure generates a system of $3N$ linear equations that can be self-consistently resolved by numerical inversion yielding the electric field $\mathbf{E}(\mathbf{r}_i, \omega_0)$ at each lattice location. In general, at this point, different observables are computed, specific either to the far-field optical response of the nanostructure (extinction or absorption cross-section ...) or to its near-field counterpart (near-field maps, near-field spectra at specific locations, ...). For instance, the extinction cross-sections computed in this paper are deduced from the self-consistent electric field at every point of the nanostructure according to [21]:

$$C_{ext} = \frac{4\pi k}{|\mathbf{E}_0|^2} \sum_{i=1}^N Im \{ \mathbf{E}_0^*(\mathbf{r}_i, \omega_0) \cdot \mathbf{P}(\mathbf{r}_i, \omega_0) \} . \quad (5)$$

In the following, we go beyond these well-known calculations and show that an extension of this numerical scheme provides direct access to the 3D charge distribution inside the nanoparticle. To achieve this objective, the polarization at every lattice point \mathbf{r}_i inside the plasmonic structure is deduced from the electric field $\mathbf{E}(\mathbf{r}_i, \omega_0)$ by applying equation (3). The volume charge density is then deduced from the polarization vector from the divergence relation:

$$\rho(\mathbf{r}, \omega_0) = -\nabla \cdot \mathbf{P}(\mathbf{r}, \omega_0) . \quad (6)$$

In order to describe the charge q_V inside a volume V delimited by the closed surface S , we apply Ostrogradsky theorem:

$$\begin{aligned} q_V(\mathbf{r}, \omega_0) &= \int_V \rho(\mathbf{r}, \omega_0) d\mathbf{r} = - \int_V \nabla \cdot \mathbf{P}(\mathbf{r}, \omega_0) d\mathbf{r} \\ &= - \oint_S \mathbf{P}(\mathbf{r}, \omega_0) \cdot \mathbf{n} d\mathbf{r} , \end{aligned} \quad (7)$$

where \mathbf{n} is a unit vector normal to S . Choosing for V a sphere of radius a passing through the closest neighbour points located on the discretization lattice, the charge density at location \mathbf{r}_i is simply given by:

$$\rho(\mathbf{r}_i, \omega_0) = -\nabla \cdot \mathbf{P}(\mathbf{r}_i, \omega_0) = \frac{3}{Na^2} \sum_{j=1}^N \mathbf{P}(\mathbf{r}_j, \omega_0) \cdot (\mathbf{r}_j - \mathbf{r}_i) \quad (8)$$

where N is the number of closest neighbours.

The latter equation allows direct calculation of the volume charge density at any point of a nanostructure from the polarization. A more limited application of our method could also directly yield the surface charge density. Here, it is important to notice that both volume charge density and surface charge density have the same physical origin. Indeed, at the boundary of a nanostructure, the presence of an abrupt interface will yield a discontinuity in dielectric constant

and polarization density. Due to this jump in polarization density, the charges on the boundary sheet of the structure will not be compensated giving large volume charge density in the surface region. Thus, the volume charge density ρ when represented as a function of the distance to the surface is an impulse function having very large values in the vicinity of a surface. From this one-dimensional singularity, the surface charge density representing the total amount of charge q per unit area can be defined. However, this mathematical abstraction should not lead to confusion: the surface charge density does not account for an additional contribution. It is not different in essence and shares the same physical origin as its volumic counterpart. In a recent paper, the resolution of Maxwell's equations in the case of arbitrarily shaped dielectrics by means of surface integral equations has been demonstrated [19]. This method involves the use of auxiliary boundary charges and currents determined by applying the appropriate boundary conditions for media separated by abrupt interfaces but, as stated by the authors, these surface charges and currents do not generally represent real interface charges. On the contrary, as will be shown in the following, our method provides direct access to the real volume charge density that is the total amount of charge per unit volume inside an arbitrarily shaped metallic nanostructure.

3. Charge distribution inside plasmonic nanoparticles: examples

3.1. Dipolar and quadrupolar surface plasmon resonances of a gold nanoprism

In the following, we apply this scheme to the identification of the multipolar modes excited by an external monochromatic plane wave light field inside a single gold nanoprism (cf. perspective view of figure (1a)). The values of the dielectric constant for gold have been taken from Johnson et al[22]. Figure (1b) begins with the typical extinction spectrum corresponding to a gold nanoprism placed in water surroundings ($\epsilon = 1.77$) and deposited on a planar silica surface ($\epsilon = 2.25$). The nanoparticle has been discretized in volume with 10829 cells ordered on a hexagonal close-packed lattice. The incident electric field is polarized along a side of the prism. This spectrum displays two optical resonances located at the wavelengths 840 nm and

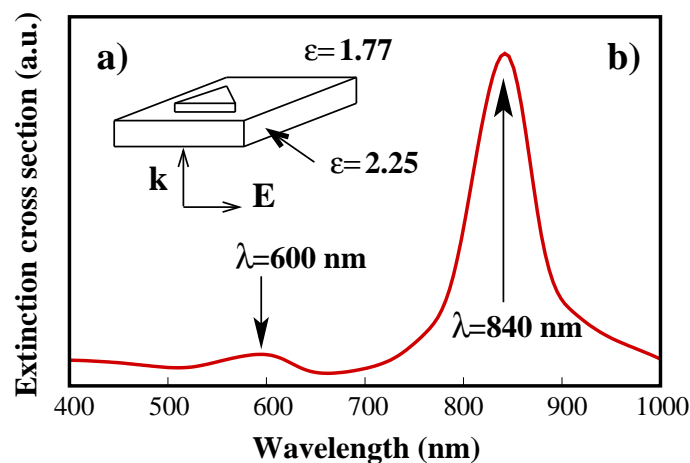


Fig. 1. (Color online) a) Perspective view of the system. The particle is a 15 nm thick gold nanoprism the section of which is an equilateral triangle of side 110 nm. b) Far-field extinction spectrum computed when the system is illuminated in normal incidence.

600 nm, respectively. Although less pronounced, the peak located around 600 nm is clearly visible. Similar spectra have already been obtained experimentally. For instance, absorption

spectroscopy experiments have evidenced two distinct plasmon resonances in colloidal silver nanotriangles [23, 24] and optical spectroscopy on lithographically fabricated gold nanoparticles [25] or colloidal gold nanoprisms [26] shows up such signatures. In a first step, we try to

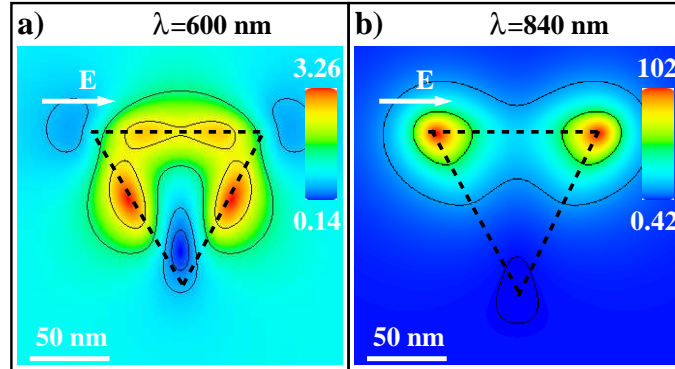


Fig. 2. (Color online) Normalized near-field optical intensity maps computed in a plane 15 nm above the nanoprism (same size as figure (1)).

get more insight in the origin of these spectral singularities by computing the near-field intensity maps that correspond to these wavelengths when the system is illuminated by an incident monochromatic field parallel to one side of the triangle.

To achieve this step, we first calculate the electric field at a location \mathbf{R} outside the nanostructure from the self-consistent field inside the metallic particles $\mathbf{E}(\mathbf{r}_i, \omega_0)$ calculated previously and the field propagator of the bare sample $\mathbf{S}_0(\mathbf{R}, \mathbf{r}_i, \omega_0)$ [20].

$$\mathbf{E}(\mathbf{R}, \omega_0) = \mathbf{E}_0(\mathbf{R}, \omega_0) + \sum_{i=1}^N \mathbf{S}_0(\mathbf{R}, \mathbf{r}_i, \omega_0) \cdot \chi(\mathbf{r}_i, \omega_0) \cdot \mathbf{E}(\mathbf{r}_i, \omega_0) \quad (9)$$

The normalized optical near-field intensity in the vicinity of the nanostructure can then be written:

$$I(\mathbf{R}) = |\mathbf{E}(\mathbf{R}, \omega)|^2 / |\mathbf{E}_o(\mathbf{R}, \omega)|^2. \quad (10)$$

Figure (2), that presents such calculations, demonstrates that important informations concerning the light confinement morphology can be extracted from the near-field intensity maps as demonstrated for instance by near-field microscopy [27]. However, it does not lead to a direct visualization of the polarization charges distribution inside the particles and only gives an indirect hint of the multipolar origin of the peaks.

As demonstrated in figure (3), the 3D mapping of the charge density, both in surface or inside the metal, allows the multipoles at work in the excited particle to be clearly identified. For the two resonances identified in the extinction spectrum, we notice that each resonance is associated with a different charge distribution. This distribution oscillates over time, and, consequently, the sign of the accumulated charges is changing every half-period. For example the map (a) in figure (3), computed for $\lambda = 840$ nm, displays a bipolar charge exchange along the nanoprism side thereby revealing a pure dipolar plasmon mode. Similarly, with four symmetrical positive and negative charge accumulations located at two corners and the two adjacent sides, the topography of the map (b) in figure (3) can unambiguously be assigned to a quadrupolar plasmon mode. Throughout the visible range, this plasmonic structure undergoes two distinct plasmonic resonances, one purely dipolar (at 840nm) and the other one involving a combination of dipolar

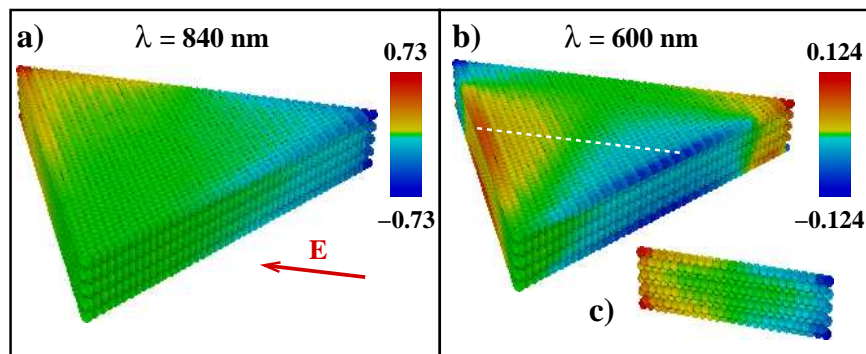


Fig. 3. (Media 1)(Color online) (Film online) Three dimensional representation of the induced charge density expressed in fC/nm^3 inside the nanoprism depicted in figure (1). The incident laser power density is $10^5 \text{ W}/\text{cm}^2$. Red and blue colors are respectively associated with positive and negative charge accumulations: (a) Map of the surface charge computed for the largest peak wavelength $\lambda = 840 \text{ nm}$; (b) Map of the surface charge computed for the second peak wavelength $\lambda = 600 \text{ nm}$; (c) A cross-section of the volume charge density performed when cutting the nanoprism along the white line of (b).

and quadrupolar components (at 600nm). In general, a purely quadrupolar mode cannot be excited from the far-field, it has indeed to be hybridized with a dipolar moment to be excited. Note that such an hybridization is allowed only if the structure does not display a 2-fold symmetry as respect to the incident polarization, like in this triangle. Finally, let us note that the near-field amplitude observed in figure (2) is directly related to the charge amount accumulated along the sides and the corners of the particle.

3.2. Charge distribution induced inside a bow-tie gold nanoantenna

Nano-antennas represent another pertinent example of interesting nanostructures. We applied our method to investigate the charge distribution inside a gold specimen composed of two equilateral triangles (size $100 \times 100 \times 20 \text{ nm}$) deposited on a glass substrate ($\epsilon = 2.25$) in air separated by a 10 nm gap. First, the extinction cross-section has been calculated (figure (4a)). An optical resonance is clearly visible at 700 nm . As in the case of a single nanoprism, we have first calculated the normalized optical near-field intensity above the object at this particular wavelength. The well-known enhancement of the electric field and spatial confinement of the electromagnetic energy in the tip region are clear on figure (4b) but the information related to the nature of the excited mode is not apparent. We have then computed the volume charge density in the metallic nanostructure at two different wavelengths for an incident electric field polarized along the interparticle axis. The figure (4c), computed at the main plasmon resonance $\lambda_d = 700 \text{ nm}$ (see extinction spectra (4a)), reveals the intense dipolar nature of the bow-tie optical response. As demonstrated by the second charge map of figure (4d), beyond this wavelength $\lambda_d = 700 \text{ nm}$, the bow-tie continues to oscillate as a dipolar mode, but with a smoother charge accumulation on the facing tips. In this second case (for $\lambda = 760 \text{ nm}$), where the spectrum displays a small shoulder, the dipolar charge distribution inside each nanoprism is very similar to the one that would be obtained in individual prisms excited at their main dipolar resonance with the same illumination configuration. Actually, this second calculation confirms that the small spectral features present in the main resonance band are not due to high order multipolar excitations as expected when working with energy lower than the dipolar mode.

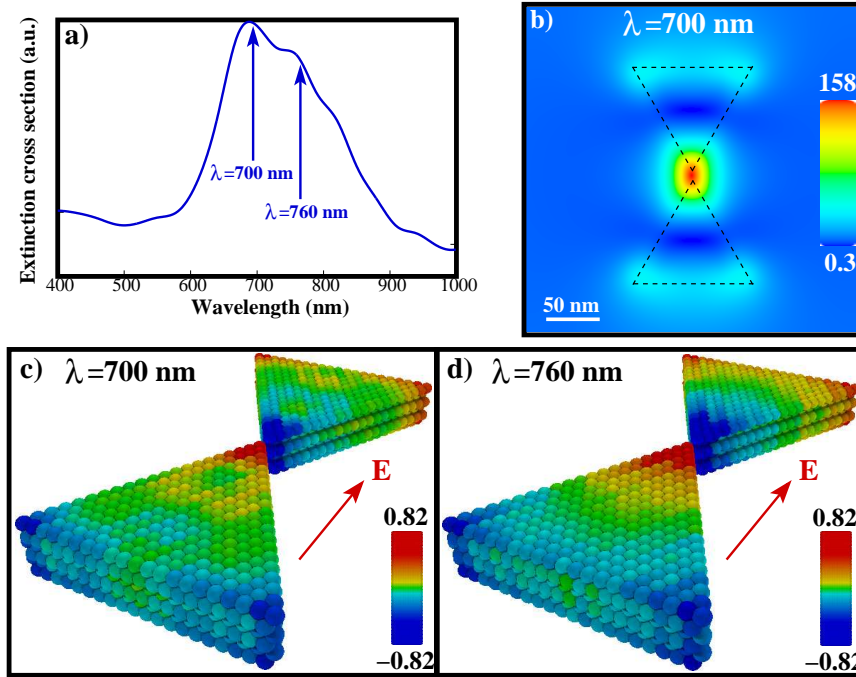


Fig. 4. (Media 2)(Color online) (Film online) a) Extinction cross-section of a gold nano-antenna composed of two equilateral triangles (100x100x20 nm) in air, deposited on a glass substrate ($\epsilon = 2.25$). b) Normalized near-field intensity map computed in a plane 15 nm above the bow-tie gold nano-antenna. c) and d) Three dimensional representations of the induced charge density expressed in fC/nm^3 inside a bow-tie gold nano-antenna for an incident laser power density of $10^5 \text{ W}/\text{cm}^2$.

4. Multipolar expansion

In molecular physics the interactions are usually expressed in terms of coupled multipolar moments[28]. In a same manner, the electronic response of plasmonic nanoparticles can be expanded as a series of electric multipoles. In plasmonics, these additional informations can be used to design structures with optimized radiative losses, for example by controlling the magnitude of the induced dipole moment. This expansion can be derived from the induced charge distribution $\rho(\mathbf{r}, \omega_0)$ applied around an arbitrary point \mathbf{r}_0 located inside the volume occupied by the metal particle[28, 29]:

$$\rho(\mathbf{r}, \omega_0) = \sum_n \frac{(-1)^n}{(2n-1)!!} \mathbf{M}^{(n)}(\omega_0) [n] \nabla^{(n)} \delta(\mathbf{r} - \mathbf{r}_0), \quad (11)$$

where, as defined in standard textbook [28, 29], $\mathbf{M}^{(n)}(\omega_0)$ denotes a multipolar moment of n th order. The zero order term of the expansion defines the net induced charge. According to the electric neutrality of the metal, this quantity vanishes for any incident wavelength. The two next contributions, namely the dipolar and quadrupolar moments, can be obtained after integration of $\rho(\mathbf{r}, \omega_0)$ over the particle volume v :

$$\mathbf{M}^{(1)}(\omega_0) = \int_v \rho(\mathbf{r}, \omega_0) (\mathbf{r} - \mathbf{r}_0) d\mathbf{r} \quad (12)$$

and

$$\mathbf{M}^{(2)}(\omega_0) = \frac{1}{2} \int_v \rho(\mathbf{r}, \omega_0) [3(\mathbf{r} - \mathbf{r}_0)(\mathbf{r} - \mathbf{r}_0) - |\mathbf{r} - \mathbf{r}_0|^2 \mathbf{I}] d\mathbf{r}. \quad (13)$$

From these equations we can define both time-dependent effective dipole and quadrupole moments associated with the metallic nanostructures:

$$\mathbf{M}^{(l)}(t) = \mathcal{M}^{(l)} \cos(\omega_0 t + \Phi^{(l)}(\omega_0)), \quad (14)$$

where $l = 1$ or 2 , and the moment magnitudes are given by

$$\mathcal{M}^{(l)}(\omega_0) = \sqrt{(\text{Re}[\mathbf{M}^{(l)}(\omega_0)])^2 + (\text{Im}[\mathbf{M}^{(l)}(\omega_0)])^2}. \quad (15)$$

The phase shift between incident field and induced moment $\mathbf{M}^{(l)}(t)$ reads:

$$\Phi^{(l)}(\omega_0) = \text{Arg}[\mathbf{M}^{(l)}(\omega_0)]. \quad (16)$$

Although our method could provide the complete multipolar expansion associated with a given physical system, we have restricted our analysis to the numerical study of the spectral variations of both dipole and quadrupole moments induced by a incident plane wave in the nanoprism of figure (1). As previously (cf. figures (2) and (3)), the incident light is polarized along a side of the prism and the reference point \mathbf{r}_0 is located in the vicinity of the triangle side parallel to the electric field. As shown in figure (5a), the magnitude of the effective dipole moment $\mathcal{M}^{(1)}(\omega_0)$,

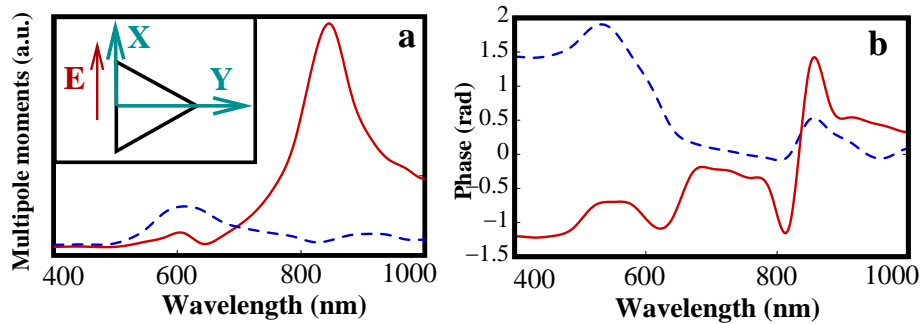


Fig. 5. (Color online) (a) Spectral variations of dipole (red line) and quadrupole (blue line) moments induced inside the nanoprism considered in figure (1). (b) Corresponding phase shifts variation versus the incident wavelength.

which is independent of the reference point for a neutral structure, displays a large peak around the 840 nm *plasmon resonance* identified in the extinction spectrum of figure (1). As illustrated in Figure (5b), we notice that the induced dipole oscillates in phase with the incident field near the resonance peak. This behavior is consistent with the theory of harmonic oscillators. Its magnitude provides a direct estimation of the coupling of the electron oscillation inside the nanostructure to the far-field incident electromagnetic wave.

The blue curves of figure (5) represent the induced quadrupole features (magnitude and phase). Formally, the induced quadrupole is a symmetric dyadic tensor defined with nine components and a *zero trace*. Due to the particular symmetry of the system, namely a triangle excited by a vector field (see inset figure (5a), only both (XY) and (YX) components of the quadrupole survive. The magnitude of the component $\mathcal{M}_{xy}^{(2)}(\omega_0)$ is represented in figure (5a) where it displays the 600 nm *plasmon resonance* identified in the extinction spectrum of figure (1).

5. Conclusion

In summary, we have developed a theoretical scheme allowing three-dimensional computation of the charge density inside arbitrarily complex plasmonic nanoparticles. The ability of the method to bring important information has been demonstrated in the case of a gold nanoprisms where both dipolar and quadrupolar volume charge distributions have been evidenced. In the case of a bow-tie gold nanoantenna, intense and opposite charge distributions accumulate at the facing tips when the field is polarized along the main axis. Finally, we demonstrate that the evaluation of the multipole moment magnitudes corresponding to a given charge distribution can be achieved with our real space approach.

Acknowledgments

This work was supported by the computing facility center CALMIP of the University Paul Sabatier of Toulouse (France).